INSTITUTE OF PHYSICS PUBLISHING JOURNAL OF PHYSICS D: APPLIED PHYSICS

J. Phys. D: Appl. Phys. **39** (2006) 5054–5063 doi:10.1088/0022-3727/39/23/023

Size-dependent creep behaviour of plasma-enhanced chemical vapour deposited silicon oxide films

Zhiqiang Cao and Xin Zhang[1]

Department of Manufacturing Engineering, Boston University, 15 Saint Mary's Street, Brookline, MA 02215, USA

E-mail: xinz@bu.edu

Received 2 June 2006, in final form 21 September 2006
Published 17 November 2006
Online at stacks.iop.org/JPhysD/39/5054

Abstract

The time-dependent plastic deformation (creep) behaviours of both as-deposited and annealed plasma-enhanced chemical vapour deposited (PECVD) silicon oxide (SiO_x) films were probed by nanoindentation load relaxation tests at room temperature. Our experiments found a strong size effect in the creep responses of the as-deposited PECVD SiO_x thin films, which was much reduced after rapid thermal annealing. Based on the experimental results, the deformation mechanism is depicted by the 'shear transformation zone' (STZ)-based amorphous plasticity theories. The physical origin of the STZ is elucidated and linked with the shear banding dynamics. It is postulated that the high strain gradient at shallow indentation depths may be responsible for the reduction in the stress exponent $n = \partial\log(\text{strain rate})/\partial\log(\text{stress})$, characteristic of a more homogeneous flow behaviour.

(Some figures in this article are in colour only in the electronic version)

1. Introduction

Plasma-enhanced chemical vapour deposited (PECVD) silicon oxide (SiO_x) thin films have been widely used in MEMS (micro-electro mechanical systems) to form both electrical and mechanical components [1]. Specifically, in power MEMS (micro energy-harvesting devices such as micro heat engines and related components) [2], PECVD SiO_x serves as an insulation layer, and endures a high level of stress even at low temperatures [3]. Severe plastic deformations in PECVD SiO_x thin films often occur, which cause device degradation or prohibit process integration [3]. So far, however, the plastic responses of the PECVD SiO_x, especially at low temperatures, have not been well understood. We are particularly interested in studying the time-dependent plastic deformation, or creep, behaviour of PECVD SiO_x, which is related to the long-term reliability issues in its applications in MEMS.

Depth-sensing instrumentation, or nanoindentation, is a popular technique for the estimation of mechanical properties of materials down to the nanoscale. It can reveal a wealth of detailed information about the mechanisms and mechanics of the studied thin film materials, including elastic modulus, hardness, surface adhesion, creep and stress relaxation behaviours, etc [4–10].

In this paper, creep responses of both the as-deposited and annealed PECVD SiO_x films were probed by the nanoindentation load relaxation experiments at room temperature. As a comparison, a standard fused quartz sample was also tested under the same conditions. In the as-deposited PECVD SiO_x thin films, our experiments found a strong size effect in the nanoindentation creep responses, which is characterized by variations in the steady-state stress exponent, $n = \partial\log(\text{strain rate})/\partial\log(\text{stress})$. Furthermore, this size effect was much reduced for both the annealed PECVD SiO_x thin film and the fused quartz. The deformation mechanisms of the various nanoindentation creep processes are depicted by the 'free volume' and 'shear transformation zone' (STZ) based amorphous plasticity theories [11–15]. The physical origin of the STZ is elucidated and linked with the shear banding dynamics. It is postulated that the high strain

[1] Author to whom any correspondence should be addressed.

gradient at shallow indentation depths may be responsible for the reduction in the stress exponent, characteristic of a more homogeneous flow behaviour. We also propose that the increase of the dispersed quasicrystal-like order in the annealed film may contribute to a more localized flow behaviour than its as-deposited counterpart.

It is well known that the plastic responses of many polycrystalline thin film materials are dependent on geometrical and microstructural lengths scales [4]. However, the size dependence in amorphous plasticity is not nearly as well studied or understood. Therefore, it is our hope that the experimental results and theoretical interpretations in the paper will not only contribute to a better understanding of the plastic behaviours of the PECVD SiO_x thin films but also provide valuable insights into the time-dependent plastic responses of other CVD materials, (such as SiN_x), physical vapour deposited (PVD) materials (such as AlO_x), and low-k silsesquioxane-based materials [3].

2. Experimental details

A 2 μm-thick, silane-based PECVD SiO_x film was deposited using a Concept One^{TM} five-station continuous plasma processing system (from Novellus Systems Inc., San Jose, CA) at 400 °C. The thin film was deposited on the front (polished) side of a 6 in. diameter, 625 μm-thick, n-type ⟨100⟩ silicon wafer, by the following reaction:

$$SiH_4 \uparrow + 2N_2O \uparrow \xrightarrow{\text{RF}}{\Delta} SiO_2 \downarrow + 2N_2 \uparrow + 2H_2 \uparrow . \quad (1)$$

The nominal gas flow rates of SiO_x were 300 sccm (sccm denotes cubic centimeter per minute at STP) of SiH_4, 9500 sccm of N_2O and 1500 sccm of N_2. The wafer was subsequently diced into approximately 10 mm × 10 mm squares. Before testing, some samples were annealed in an RTP-600S rapid thermal annealing (RTA) system (from Modular Process Technology Corp., San Jose, CA) for 10 min at 800°C in a nitrogen environment. All the references of the 'annealed film' in the rest of the paper refer to the PECVD SiO_x films that were treated by RTA described above.

The nanoindentation tests were conducted at room temperature on a TriboIndenter^{TM} system (from Hysitron Inc., Minneapolis, MN), which is capable of high-rate, high-resolution measurements. The vertical load resolution of the nanoindentation system is 1 nN, with a noise floor of 100 nN, and the vertical displacement resolution is 0.04 nm, with a noise floor of 0.2 nm. A standard Berkovich tip was used, with a pyramidal tip shape and a tip radius of approximately 150 nm. Both the machine compliance and the tip area functions were carefully calibrated on a standard fused quartz sample (also from Hysitron Inc.), following the procedure proposed by Oliver and Pharr [5]. Separate area functions were calibrated for different ranges of loads to ensure good fits at all depths.

Prior to each test, efforts were made to minimize the effects of the thermal drift by allowing thermal equilibrium to be reached for more than one hour. Consequently, the thermal drift became steady and typically could reach 0.01 nm s^{-1} or less. Compensations were then automatically made to correct the data.

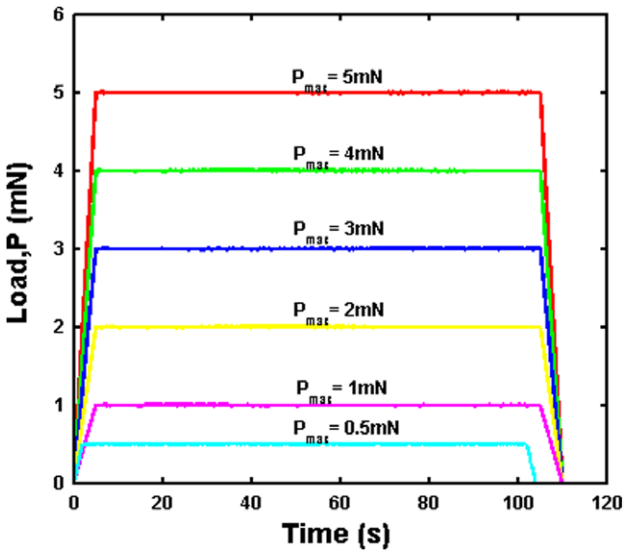

Figure 1. Load scheme of the indentation load relaxation (ILR) experiments.

Indentation load relaxation (ILR) tests were separately performed on the as-deposited PECVD SiO_x, annealed PECVD SiO_x and the fused quartz samples, all in a load-controlled mode and under a constant peak load ranging from 500 to 5000 μN. The holding time was 100 s in all the experiments, as shown in the load scheme (figure 1). Each test was repeated at least five times under the same loading condition for each sample.

For our PECVD SiO_x thin films samples (both as-deposited and annealed), when the peak load was 5 mN, the maximum indentation depth was less than 300 nm, or 15% or the film thickness. Thus, the influence of the silicon substrate effects should have been minimal [16].

3. Data analysis

For a given material, different creep mechanisms may be operative at different temperatures and stress levels. To gain more insights into the time-dependent properties of the sample materials, it is desirable to obtain the relationship between the nanoindentation strain rates ($\dot{\varepsilon}_I$) and the average indentation stress $\bar{\sigma}$ during the holding time. In the uniaxial tests, the steady-state behaviour of a wide range of materials can be expressed by

$$\frac{\dot{\varepsilon}}{\dot{\varepsilon}_0} = \left(\frac{\sigma}{\sigma_0}\right)^n , \quad (2a)$$

in which $\dot{\varepsilon}_0$ and σ_0 are material parameters. In general, a non-dimensional form such as equation (2a) is preferred in the theoretical analysis. However, in the experimental characterizations, we find it is more convenient to use the following revised form:

$$\dot{\varepsilon} = A\sigma^n \quad (2b)$$

in which A is a material parameter and

$$A = \left(\frac{\dot{\varepsilon}_0}{\sigma_0}\right)^n . \quad (2c)$$

In the conventional uniaxial creep tests, either the stresses or the strain rates are kept constant. Indentation creep tests, however, are different with traditional uniaxial tests in several ways. First, the stresses generated in an indentation test include compressive, tensile, and shear stresses in all directions. The strain rates experienced in an indentation test are also much more complex and may cover a wide range, especially at the beginning of the indentation [8]. Despite all the differences, a number of previous theoretical and experimental studies have found that it is possible to link the results of indentation to those obtained from the uniaxial tests [17–20]. Tabor [17] first proposed an empirical 'equivalent strain' concept, which was validated by Bower *et al* [18] through both rigorous theoretical modelling and finite element analysis. Storåkers and Larsson [19] extended the work of Hill [20] on the contact mechanics of the indentation process and also determined that the indentation creep could be defined by an equivalent indentation strain rate. These results generally show that for Berkovich (and other self-similar) tips, the indentation strain rate $\dot{\varepsilon}_{\mathrm{I}}$ scales as

$$\dot{\varepsilon}_{\mathrm{I}} \sim \frac{1}{h}\frac{\mathrm{d}h}{\mathrm{d}t}. \tag{3}$$

In our indentation load relaxation experiments, equation (3) is applied at relatively large indentation depths, where the displacement rate is small compared with the beginning of indentation. As Poisl *et al* pointed out [8], in such a case, the concept of an equivalent strain rate may be valid.

In addition to the equivalent strain/strain rate, it is found that most of the material underneath the indenter is subjected to a constant level of equivalent stress, approximated by the mean pressure that can be sustained under the indentation load. In other words, we can also define a single representative or 'equivalent stress' together with an 'equivalent strain/strain rate' during the indentation process.

In equation (3), h is the indentation depth, and t is the time. $\mathrm{d}h/\mathrm{d}t$ is calculated by first fitting the h–t curve during holding with the empirical law [21]:

$$h(t) = h_0 + a(t - t_i)^b + kt, \tag{4}$$

where t_i is the time when the creep process is initiated. h_0 (close to h_i, the initial indentation depth) , a, b and k are constants obtained from fitting equation (4) to the h–t curves. We did not assign physical meanings to these fitting parameters, as equation (4) is empirical in nature. As we will show later, equation(4) fits most of the results very well, with $R^2 > 0.95$ or better.

At very small depth, the shapes of the pyramidal tips and conical tips are rounded. For these tips, the maximum contact depth below which the indent shape is spherical can be estimated by [21]

$$\delta_0 = R(1 - \sin\beta), \tag{5}$$

where β is the semiangle of the indenter tip, and R is the tip radius. δ_0 is approximately 14 nm for our Berkovich tip, whose $\beta = 65.35°$. All our experimental results in this paper were obtained at indentation depths far greater than 14 nm.

Many applications of the instrumented indentation are limited by the complications in clearly interpreting the results.

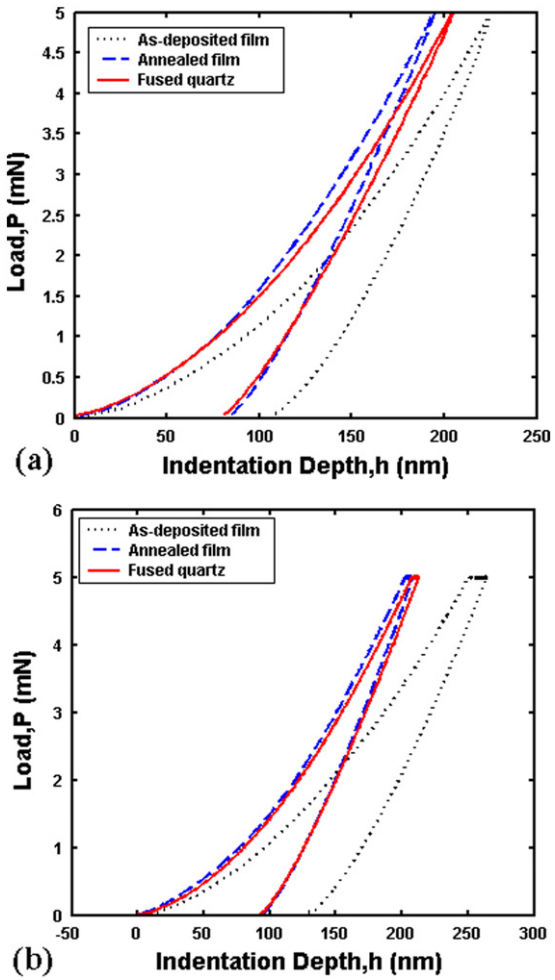

Figure 2. Load-displacement (P–h) relations of the (a) constant rate of loading (loading/unloading times: 2 s) and (b) indentation load relaxation experiments with a maximum load ($P_{\max}$) of 5 mN.

Such complications arise mainly from the 'pile-up' or 'sink-in' of the material around the indenter [6]. Figure 2 shows the load–displacement (P–h) relations of the constant rate of loading (loading/unloading times: 2 s) and ILR experiments with a maximum load ($P_{\max}$) of 5 mN. In our experiments, the indentation depths were small (<300 nm), and from figure 2(a) $h_{\mathrm{f}}/h_{\max} < 0.7$, where h_{f} is the final indentation depth, and h_{max} is the maximum indentation depth. Therefore, theoretically the 'pile-up' should have been negligible [6]. This assumption was proven experimentally by the *in-situ* scanning probe microscopy (SPM) images which used the indenter itself as the imaging tip. For example, figure 3 is a complete (inverse) 3D image showing the topography and the curvature of the faces after an indent on the standard fused quartz sample. Figure 4 demonstrates both the top view and a cross section line profile of the same indent as in figure 3. During loading, both elastic and plastic deformation processes occur, and the indenter conforms perfectly to the pyramidal shape of the hardness impression. During unloading, however, the elastic recovery causes the hardness impression to change its shape, as accentuated by the (red) dashed straight lines in figure 4(b) [6]. Similarly, typical residual indents of the as-deposited and annealed PECVD SiO_x films were shown in

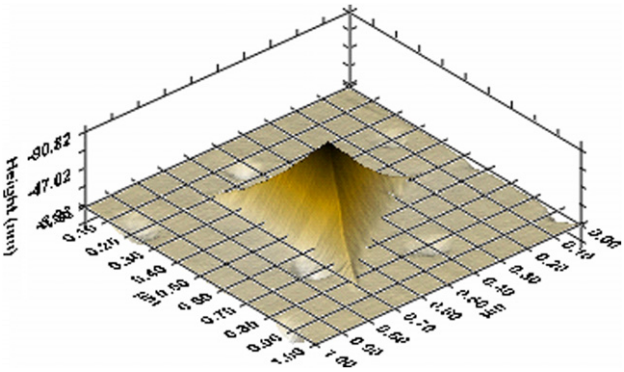

Figure 3. A complete (inverse) 3D image showing the curvature of the faces after an indent on the standard fused quartz sample (ILR experiment, $P_{max} = 5$ mN).

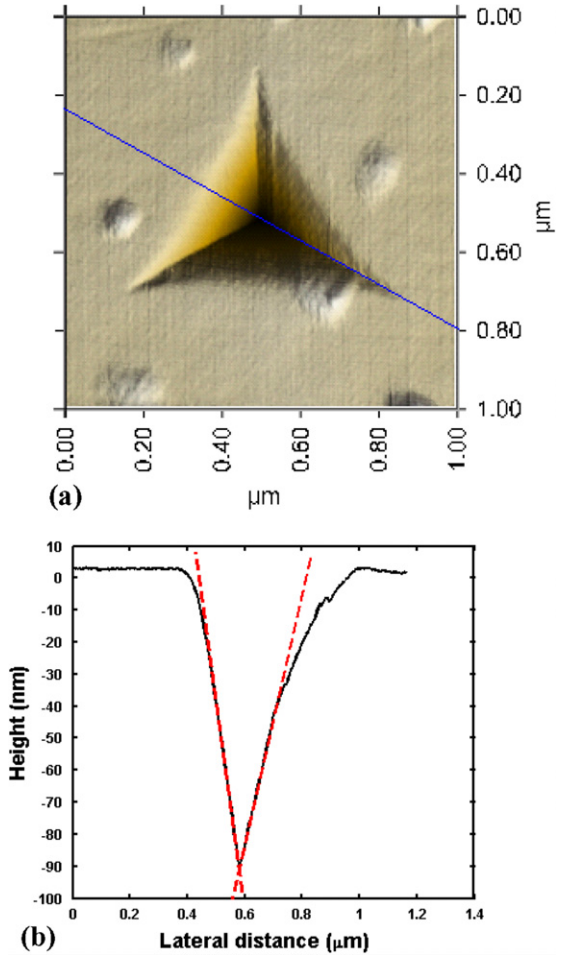

Figure 4. (*a*) The 3D top view and (*b*) Cross section line profile (through an edge and opposing face) of indent on the standard fused quartz sample (ILR experiment, $P_{max} = 5$ mN).

figure 5. It can be directly observed from the SPM images such as figures 3–5 that the 'pile-up', if any, was negligible in all the tested sample materials. Thus the creep behaviours in our experiments were induced by plasticity. As such, the uncertainty of the contact area–indenter depth relation is reduced by suppression of the 'pile-up'.

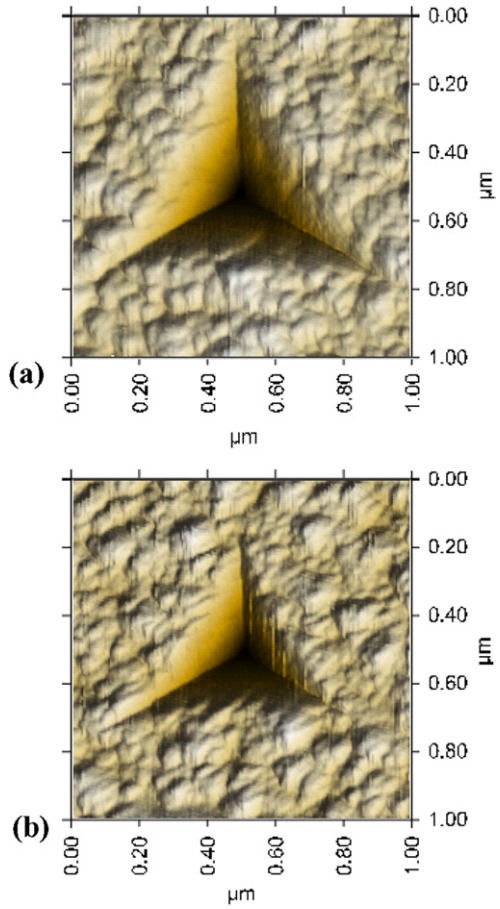

Figure 5. *In-situ* SPM images of residual prints of (*a*) as-deposited and (*b*) annealed PECVD SiO_x films (ILR experiment, $P_{max} = 5$ mN).

The 'sink-in' was primarily caused by the elastic deflection of the specimen surface, and the relation $h_c = f(h)$ between contact depth (h_c) and the measured instant maximum depth (h) was calibrated before the experiments. In our experiments, we found that $h_c = f(h)$ is approximately linear, as predicated by theory [5, 6]. By examining a wide range of different loading/holding conditions, we also found that the variations of f are small and well within the $\pm 5\%$ error range typically associated with nanoindentation measurements [6]. Knowing $h_c = f(h)$ and the area function of the nanoindenter tip $A = F(h_c)$, it is possible to evaluate also the instant hardness H in a creep process following

$$H = \frac{P}{A}. \tag{6}$$

Note that H also signifies the mean pressure, or the average stress $\bar{\sigma}$, that can be sustained under the indentation load [4].

4. Experimental results

Significant creep displacements were observed in all the samples during the holding time of the ILR tests. The relations between the creep displacement (h–h_i) and creep time (t–t_i) for the three materials under different peak loads (P_{max}) are plotted by the coloured dots in figures 6(*a*)–(*c*). The smooth black

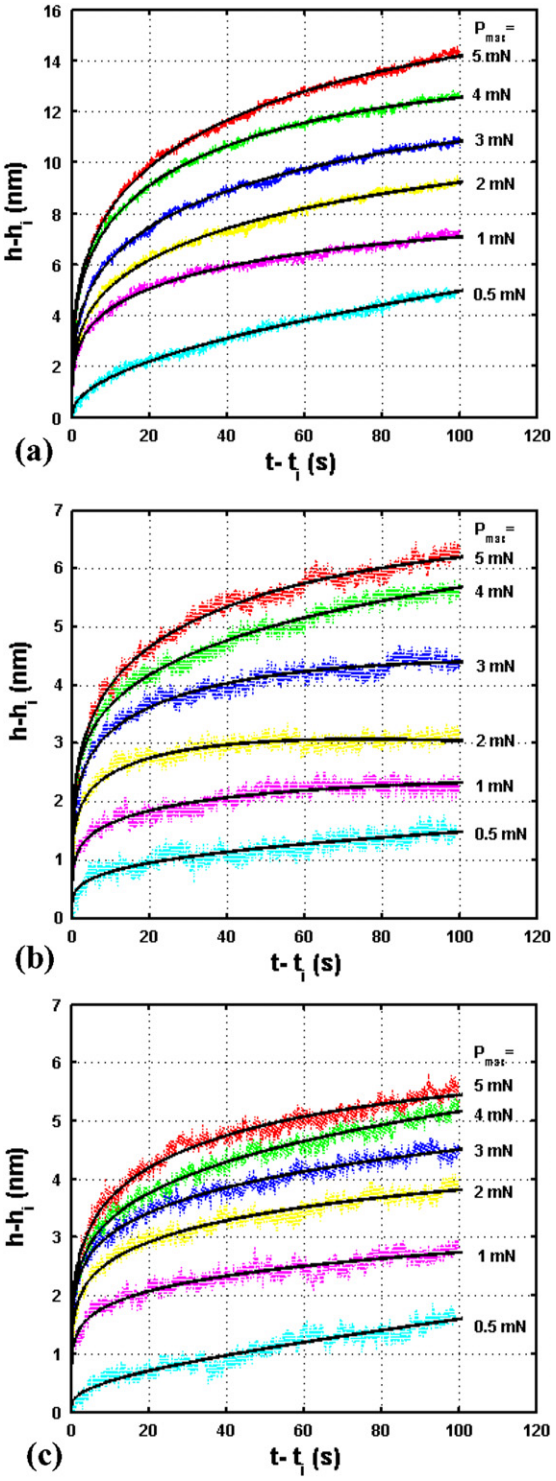

Figure 6. The experimental data (coloured dots) and fitting (black lines) of the creep displacement (h–h_i) versus hold time (t–t_i) relations of (*a*) the as-deposited PECVD SiO_x film (*b*) annealed PECVD SiO_x film, and (*c*) fused quartz under different peak loads (P_{max}).

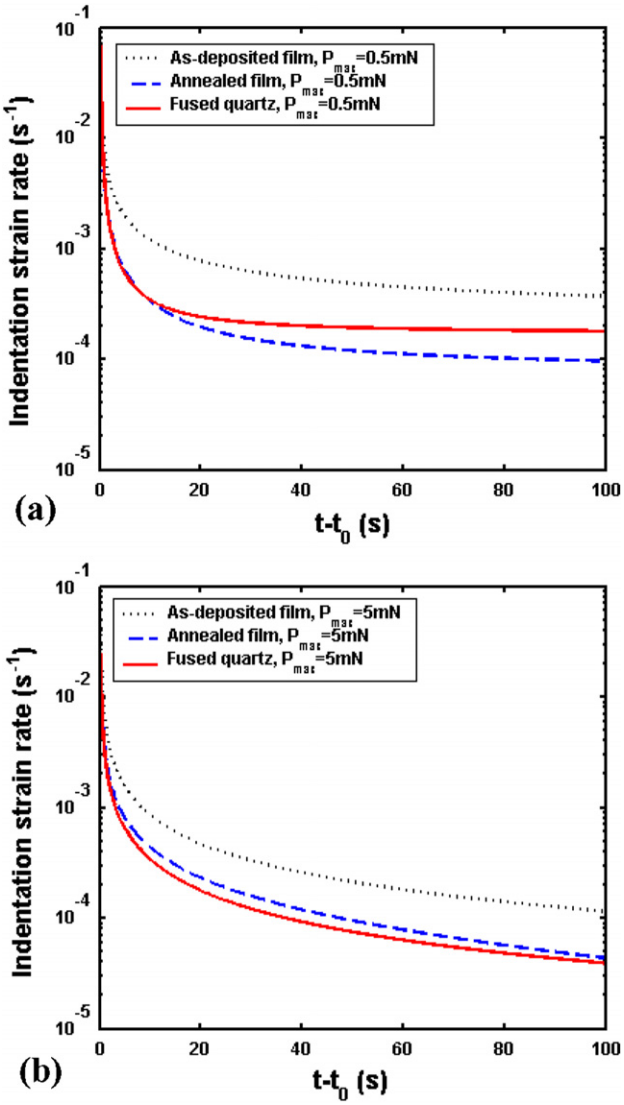

Figure 7. The $\dot{\varepsilon}_I \sim (t - t_0)$ (indentation strain rate versus creep time) relations of the three sample materials under (*a*) 500 μN and (*b*) 5 mN constant peak loads.

solid lines represent the respective fittings by equation (4). It can be seen that for the larger peak loads, its total creep displacement is relatively larger.

The creep rate (strain rate during creep) $\dot{\varepsilon}_I$ and the stress $\bar{\sigma}$, both during the holding time, were calculated from equation (3) and equation (6), respectively. It is found that $\dot{\varepsilon}_I$ declines with time, as shown in figures 7(*a*)–(*b*), reaching approximately a steady state as the displacement rate $\mathrm{d}h/\mathrm{d}t$ decreases. Obviously, $\bar{\sigma}$ also decreases with time as the creep displacement (and thus the projected area) increases. Comparing figures 7(*a*) and (*b*), it is also apparent that the strain rate at small indentation depths is relatively larger than that of the deeper indentation depths.

Figures 8(*a*) and (*b*) are the $\log \dot{\varepsilon}_I$–$\log \bar{\sigma}$ relations of the as-deposited PECVD SiO_x films under the minimum (500 μN) and maximum (5 mN) constant peak loads. The slopes of both the curves, i.e. $n = \partial(\log \dot{\varepsilon}_I)/\partial(\log \bar{\sigma})$, drop significantly as the creep displacement increases and stress decreases. Evidently, with the smaller indent this reduction in the slopes is faster. At the steady state (i.e. toward the end of the holding time), n represents the stress exponent of a power-law creep [7, 8], and will be analyzed further for a better understanding of the creep process. It is apparent from figures 8(*a*) and (*b*) that for very shallow indents, the steady-state stress exponent

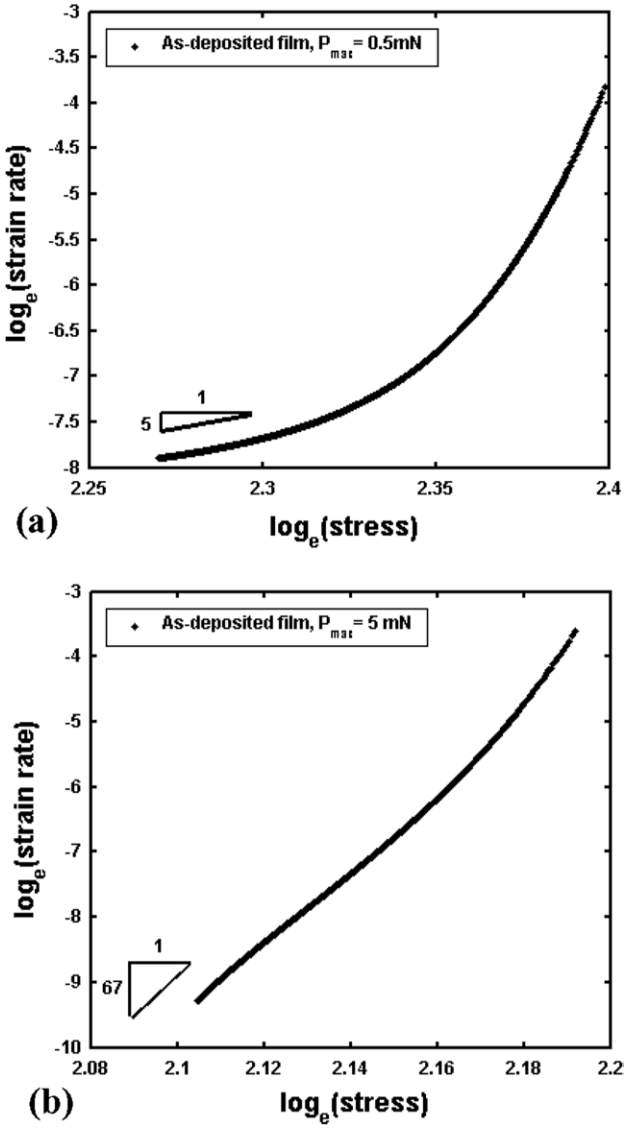

Figure 8. The $\log \dot{\varepsilon}_I - \log \bar{\sigma}$ relations of the as-deposited films under (*a*) 500 μN and (*b*) 5 mN constant peak loads.

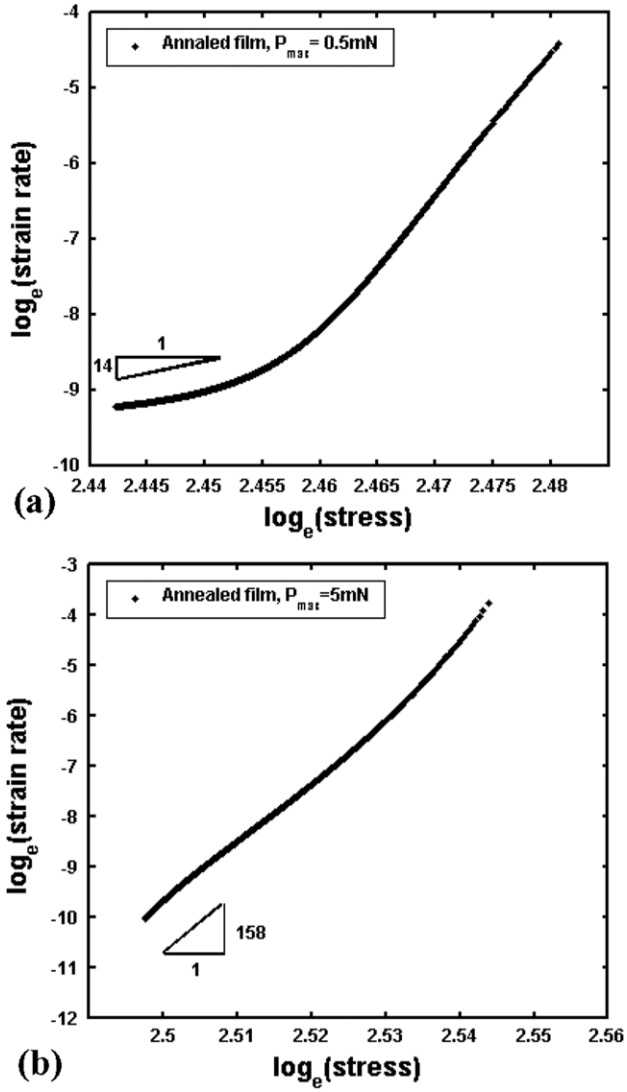

Figure 9. The $\log \dot{\varepsilon}_I - \log \bar{\sigma}$ relations of the annealed films under (*a*) 500 μN and (*b*) 5 mN constant peak loads.

n is on the order of unity (∼5). As the load increases ten times, n increases quite dramatically (to ∼67). The above observations, including the size effects in stress exponents in figures 8(*a*) and (*b*), are qualitatively the same for the annealed PECVD SiO_x thin film and the fused quartz samples, whose related results are shown in figures 9–10 for comparison. In figures 8(*b*) and 9(*b*), it appears to us that the slight increase in slopes near the end of holding time might be caused by substrate deformation, as at such large loads, the penetration depth has already slightly exceeded 10% of the film thickness (2 μm). But as this influence is not significant, we chose to focus on the larger trend of the data.

Finally, figure 11 shows the variations of stress exponent values at the end of holding time, as a function of peak load for three different sample materials. The nominal initial indentation depths at the various loads are tabulated in table 1. After RTA, the stress exponents of the PECVD SiO_x films are generally much increased under comparable loading conditions. In addition, it is evident that the stress exponents of all the sample materials exhibit a strong size effect at the smallest indentation depth, with a value on or approaching the order of unity. As the load and indentation depth increases, n quickly saturates into a large value of ∼150 for the annealed film. For the fused quartz sample, it also shows a sign of saturation within the tested range. However, as for the as-deposited film, no similar trend is yet observed within the 5 mN range.

The different size effects in the stress exponent values of the tested samples may suggest there is a difference in their deformation mechanisms during creep. To understand the phenomena better, we also measured the hardness (equivalent to average stress) values of different samples, as shown in figure 12. After RTA, the hardness of the PECVD SiO_x thin film is increased to a value close to that of fused quartz. There are, however, no significant size effects in hardness in the annealed film and the fused quartz within the same load range. For the as-deposited PECVD SiO_x film, a small but noticeable size effect can be observed at small peak loads. At larger loads, the hardness values do not vary significantly. In any case, the

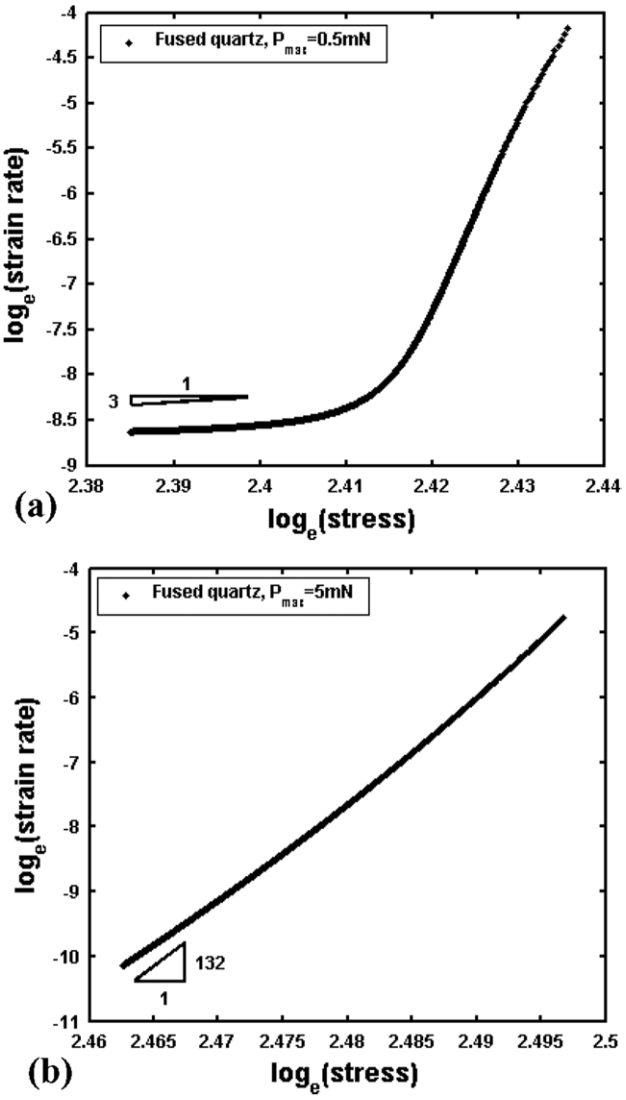

Figure 10. The $\log \dot{\varepsilon}_I$–$\log \bar{\sigma}$ relations of the fused quartz under (*a*) 500 μN and (*b*) 5 mN constant peak loads.

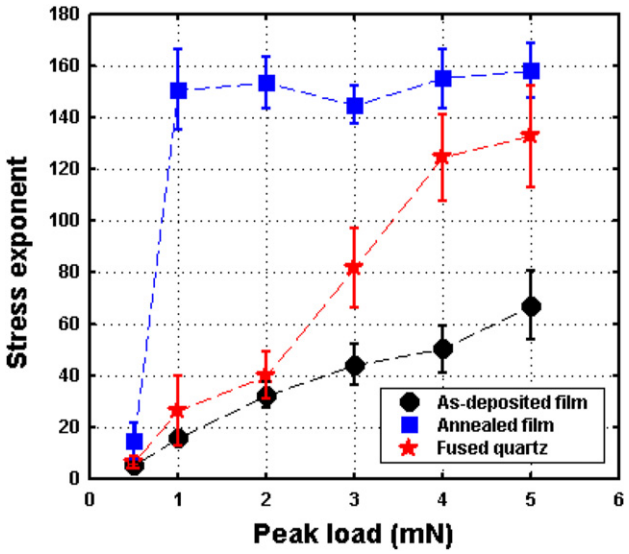

Figure 11. Steady-state stress exponent as a function of peak loads for different sample materials.

size effects in stress exponent in figure 11 seem hardly directly correlated with the size effects in hardness, shown in figure 12.

5. Discussion

Indentation size effects (ISE) are mostly found in both microhardness and nanohardness tests of crystalline/polycrystalline materials [22–24]. Although the underlying mechanisms remain irresolute, a 'strain gradient plasticity (SGP)' theory has been successfully applied to explain a wide range of experiments [23,24]. This theory proposes that the large strain gradient inherent in small indents leads to 'geometrically necessary dislocations' that cause enhanced hardening. When the grain size decreases to the nanometre range, i.e. in nanocrystalline solids, enhanced size effects and strain rate sensitivity are often observed and attributed to the presence of a large density of grain boundaries (GB) [25–27].

The occurrences of plastic deformation in all of our sample materials were confirmed by both the nanoindentation load–displacement (P–h) curves and the SPM images of residual indent prints such as in figure 2 and figures 3–5. Thus, the creep behaviours observed in section 4 were apparently induced by plasticity.

Due to their fabrication methods, both the fused quartz and the PECVD SiO_x are known to be amorphous. Generally speaking, in amorphous solids, the physical process of plastic deformation differs substantially from those of the crystalline, polycrystalline and nanocrystalline materials. Clearly identifiable defects, such as dislocation and GB, cease to provide a useful description of the microstructural dynamics [14]. In the most widely accepted theory of amorphous plasticity, Spaepen, Argon [11,12] and others have shown that at low temperature and high stress, the flow is inhomogeneous and plastic deformation occurs at localized sites (called flow defects) in the form of 'shear bands'. Falk, Langer and others [13–15] have further built on such models and proposed that the deformation is mediated by the activation of the rearrangement of a particularly oriented cluster of atoms, known as shear transformation zones (STZs).

As a result of the PECVD process, a large density of the Si–O bonds in the as-deposited PECVDSiO_x is either distorted (i.e. compressed or stretched) or dangling/broken (such as–SiO_3 bonds), forming defects. In addition, our previous SIMS (second ion mass spectroscopy) analysis found that there was a significant hydrogen concentration near the free surface of the film (∼6.7%), which decreased to ∼2% at about 500 nm from the free surface [3]. Due to the RF plasma environment, the incorporated hydrogen atom is likely to be ionized and enters into the Si-O network, forming Si-OH bonds. After thermal annealing, this hydrogen concentration is dramatically reduced (to a relatively constant level of ∼0.1% at all depths). The hardness of the film is increased (shown in figure 12), as the defect density is reduced and a relatively more orderly microstructure results.

In the STZ theory of amorphous plasticity, a large n (for example, $n > 100$) implies that the flow is inhomogeneous. In

Table 1. Initial indentation depths (nm) at various loads in different samples.

Nominal P_{max} (mN)	0.5	1	2	3	4	5
As-deposited	57.552	99.067	149.71	184.39	215.21	250.68
Annealed	54.773	84.08	125.03	145.58	181.53	202.76
Fused quartz	56.628	83.674	122.35	153.36	182.61	207.47

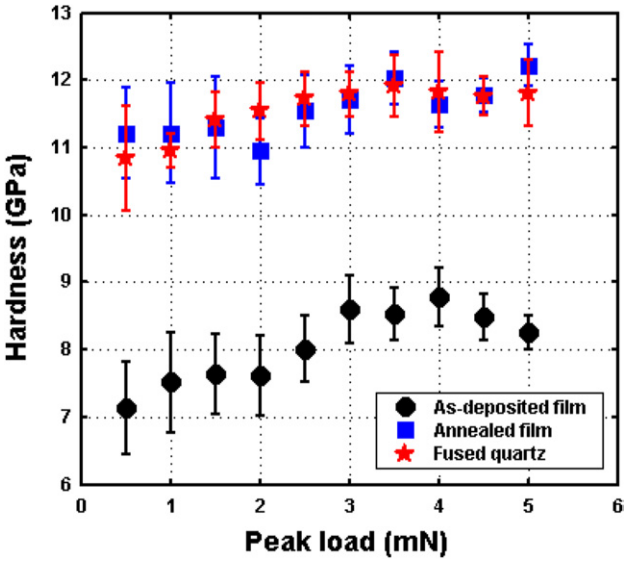

Figure 12. Hardness values of different sample materials under various peak loads.

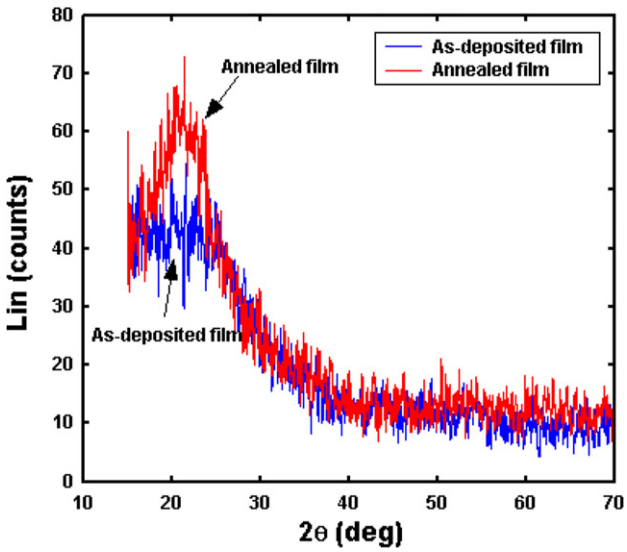

Figure 13. X-ray diffractograms for both the as-deposited and 800 °C RTA annealed PECVD SiO_x thin film samples.

other words, it is characteristic of an instability behaviour—that the STZ clusters are unstable against the autocatalytic formation of large-scale shear bands, and the plastic flow is concentrated into a few such shear bands, and thus the flow becomes more inhomogeneous. On the other hand, a small n (for example, <10) implies the flow is more viscous (in the case of $n = 1$, the flow would be Newtonian viscous).

It can be inferred from figures 8–10 that, due to a high stress level, the nanoindentation creep process starts out to be almost ideally plastic, with a high stress exponent and almost rate-insensitive. This may be explained by the conventional STZ theory: when the applied stress exceeds the yield stress, the movement of a first STZ (either weak Si–O, Si–OH bonds or the dangling/broken $–SiO_3$ bonds) will cause a local dilatation or expansion of the nearby free volumes [11]. This, in turn, creates localized distortions of neighbouring STZs, and triggers the autocatalytic formation of large bands of STZs, commonly called 'shear bands' [11, 12]. Note that the shear bands formed here, although much larger than a single STZ, are still so small that they may not be detectable by techniques such as SPM (figures 3–5). Nevertheless, they will result in a local softening of the material, as the dynamic excess free volume lowers the average shear resistance of the sheared regions. Eventually, the applied strain relaxes and the growth of the bands stops due to dynamic effects or small but rapid stress drops in the vicinity of the bands [12]. Thus near the end of the holding time, we see a reduction in the stress exponent, indicating that the flow has become more homogeneous (i.e. viscous-like) than at the start.

During the nanoindentation process of a sharp wedge (including the Berkovich tip), at very shallow depths, the applied strain gradient is significantly higher than that of the deeper indents [22–24]. We postulate that this will create an extra imbalance among the STZs and promote the rate at which the shear bands form and relax underneath the indenter tip. To verify this argument, we turn to figures 7–10. Faster rates of shear band formations would result in a higher strain rate at a smaller indentation depth, which is clearly supported by figure 7. On the other hand, figures 8–10 demonstrate that the relaxation rate is much greater at the smaller indentation depths. As a result of the quick termination in growth, the shear bands generated at very shallow depths should be generally much smaller. At steady state, atomic diffusion may be enhanced as a result of a higher rate of dynamic equilibrium of the rearrangement of STZs. As such, the numerous smaller shear bands in the specimen may collectively exhibit a more macroscopically viscous-like flow behaviour, which is experimentally confirmed by a reduction in its stress exponent at shallow depths in figure 11. In other words, the length-scale effect in an amorphous material might be related to the sizes of the shear bands. When the shear bands are small and numerous, a more 'homogenous' flow behaviour will result; whereas if the shear bands are large and few, the flow behaviour will become more 'inhomogeneous'. Variations in their stress/strain distribution profiles might also play a role in determining the quantitative values of stress exponents at different loads/depths, but based on our previous discussions

on the 'equivalent stress/strain' concept, it is unlikely that such variations would affect the overall qualitative conclusions.

We further propose that the size effect in the stress exponents is much more pronounced in the as-deposited PECVD SiO_x film, mainly because (1) its defect density is higher, especially near the free surface and (2) the shear resistance of the STZs is intrinsically weaker than that of the annealed film or the fused quartz. This is based on the recent experimental evidence and simulation study that suggest the dispersed local quasicrystal-like order plays a critical role in controlling the qualitative nature of amorphous plasticity [28, 29]. Larger degrees of quasicrystal-like order tend to increase shear localization [28]. To validate this claim, we performed additional x-ray diffraction (XRD) measurements (with a D8 Focus^{TM}, from Bruker AXS Inc., Madison, WI) on both the as-deposited and annealed PECVD SiO_x thin films and the results are presented in figure 13. It can be seen that for the as-deposited film, the data does not show any clear features, confirming that the material microstructure is totally amorphous. However, after RTA, a noticeable peak can be resolved at $\sim 22^\circ$, indicating that some of the amorphous SiO_x clusters possess an increased medium-range order [30, 31]. In other words, after RTA, the microstructure becomes relatively more orderly and the 'quasicrystal-like order' increases.

It is possible that in the as-deposited PECVD SiO_x, the paucity of such 'quasicrystal-like order' may contribute to a generally less inhomogeneous flow behaviour, or a reduction in the steady-state stress exponent, as seen in figure 11. On the other hand, the increase in the dispersed quasicrystal-like order, by reducing the defects in the annealed film, may contribute to a more localized flow behaviour than its as-deposited counterpart.

Due to the depth dependence of the hydrogen content, we caution here that the clear interpretation of the results of the as-deposited films is likely to be complicated. However, the size effects in stress-exponents were also observed at small loads/depths in the annealed films, which had a constant level of hydrogen of $\sim 0.1\%$; as well as in the fused quartz, which does not contain similar defects. It is therefore argued that the size effect in this paper is a true local length-scale effect, although it can be influenced by other factors such as defect density distributions etc. Since the conventional STZ theories generally do not contain an explicit 'length scale' factor, we call for further experimental and theoretical studies into the size effects in amorphous plasticity to gain a better understanding of the underlying mechanisms.

We would like to end this paper by noting that the STZ based deformation mechanism presented in this paper is just one possible way of interpreting the experimental results. Nevertheless, this theory relies on few assumptions and does not exclude other possibilities. For example, if there is a densification or an ordering transition under the indent, it will have an influence on the character of the plastic flow. However, from the STZ point of view, the changes in the size of shear bands and STZ clusters are equivalent to the densification or order transition effects at a local scale. In this sense, the two mechanisms are not contradictory to each other.

6. Conclusions

The time-dependent plastic behaviours of both the as-deposited and annealed PECVD silicon oxide (SiO_x) films were probed by nanoindentation creep experiments at room temperature. Our experiments found a strong size effect in the creep responses of the as-deposited PECVD SiO_x thin films, which was much reduced after annealing. Based on the experimental results, the deformation mechanism is depicted by the STZ based amorphous plasticity theories. The physical origin of the STZ is elucidated and linked with the shear banding dynamics. It is postulated that the high strain gradient at shallow indentation depths may be responsible for the reduction in the stress exponent, characteristic of a more homogenous flow behaviour. We also propose that the increase in the dispersed quasicrystal-like order in the annealed film may contribute to a more inhomogeneous flow behaviour than its as-deposited counterpart.

Acknowledgments

We gratefully acknowledge the funding for this project by the Air Force Office of Scientific Research (AFOSR) under Contract No F49620-03-1-0078. The authors also thank Professor Catherine Klapperich of Boston University for her support on the nanoindentation system.

References

[1] Madou M 2002 *Fundamentals of Microfabrication: The Science of Miniaturization*, 2nd edn (Boca Raton, FL: CRC)
[2] Epstein A H and Senturia S D 1997 *Science* **276** 1211
[3] Cao Z and Zhang X 2004 *J. Appl. Phys.* **96** 4273 and references therein
[4] Freund L B and Suresh S 2004 *Thin Film Materials: Stress, Defect Formation and Surface Evolution* (Cambridge: Cambridge University Press)
[5] Oliver W C and Pharr G M 1992 *J. Mater. Res.* **7** 1564
[6] Oliver W C and Pharr G M 2004 *J. Mater. Res.* **19** 3
[7] Lucas B N and Oliver W C 1999 *Metall. Mater. Trans.* A **30A** 601
[8] Poisl W H, Oliver W C and Fabes B D 1995 *J. Mater. Res.* **10** 2024
[9] Elmustafa A A and Stone D S 2003 *J. Mech. Phys. Solids* **51** 357
[10] Schuh C A and Nieh T G 2004 *J. Mater. Res.* **19** 46 and references therein
[11] Spaepen F 1977 *Acta. Metall.* **25** 407
[12] Argon A S 1979 *Acta. Metall.* **27** 47
[13] Falk M L and Langer J S 1998 *Phys. Rev.* E **57** 7192
[14] Langer J S 2001 *Phys. Rev.* E **64** 011504
[15] Falk M L, Langer J S and Pechenik L 2004 *Phys. Rev.* E **70** 011507
[16] Bhattacharya A K and Nix WD 1988 *Int. J. Solids Struct.* **24** 1287
[17] Tabor D 1951 *The Hardness of Metals* (Oxford: Clarendon)
[18] Bower A F, Fleck N A, Needleman A and Ogbonna N 1993 *Proc. R. Soc. Lond.* A **441** 97
[19] Storåkers B and Larsson P L 1994 *J. Mech. Phys. Solids* **42** 307
[20] Hill R 1992 *Proc. R. Soc. Lond.* A **436** 617
[21] Li H and Ngan A H W 2004 *J. Mater. Res.* **19** 513
[22] Tymiak N I, Kramer D E, Bahr D F, Wyrobek T J, and Gerberich W W 2001 *Acta. Mater.* **49** 1021

[23] Nix W D and Gao H 1998 *J. Mech. Phys. Solids* **46** 411
[24] Fleck N A and Hutchison J W 2001 *J. Mech. Phys. Solids* **49** 2245
[25] Schwaiger R, Moser B, Dao M, Chollacoop N, and Suresh S 2003 *Acta Mater.* **51** 5159
[26] Lu L, Sui M L and Lu K 2000 *Science* **287** 1463
[27] Schiøtz J, Di Tolla F D, and Jacobsen K W 1998 *Nature* **391** 561
[28] Shi Y, Falk ML 2005 *Appl. Phys. Lett.* **86** 011914
[29] Saksl K, Franz H, Jóvári P, Klementiev K, Welter E, Ehnes A, Saida J, Inoue A, and Jiang J Z 2003 *Appl. Phys. Lett.* **83** 3924
[30] Gaskell G H and Wallis D J 1996 *Phys. Rev. Lett.* **76** 66
[31] Comedi D, Zalloum O H Y, Irving E A, Wojcik J, Roschuk T, Flynn M J, and Mascher P 2006 *J. Appl. Phys.* **99** 023518